CASE FILE
COPY

N71-32323
NASA TM X-67886

NASA TECHNICAL MEMORANDUM

NASA TM X-67886

OPTIMAL ROUND TRIP SPACE TUG TRAJECTORIES FOR EARTH ESCAPE MISSIONS

by Vernon J. Weyers and Fred Teren
Lewis Research Center
Cleveland, Ohio

TECHNICAL PAPER proposed for presentation at
Astrodynamics Specialists Conference sponsored by the
American Astronomical Society and the American
Institute of Aeronautics and Astronautics
Fort Lauderdale, Florida, August 17-19, 1971

OPTIMAL ROUND TRIP SPACE TUG TRAJECTORIES

FOR EARTH ESCAPE MISSIONS

by Vernon J. Weyers and Fred Teren

National Aeronautics and Space Administration
Lewis Research Center
Cleveland, Ohio

E-6478

ABSTRACT

Optimum round trip trajectories for reusable space tug payload injection missions at energy levels above Earth escape are determined. The variational maximum principle is used to formulate and solve the mathematical problem. Solutions of the resulting two point boundary value problem are obtained by numerical integration and finite difference Newton-Raphson iteration techniques. A method for obtaining approximate solutions of the mathematical problem is also presented. The approximate solutions are much easier to obtain than the exact ones and the results are in excellent agreement. Details of the mathematical analysis are included.

Payload capability is presented as a function of the injection energy. The effects of finite thrust level, vehicle turn-around time, and total trip time are included. Results are shown for various values of stage propellant mass fraction and specific impulse. Characteristics of the optimum trajectories are discussed.

INTRODUCTION

Long range NASA plans include development of a Reusable Space Tug (RST). The RST may be capable of either Earth-based or space-based operation and will be used for a wide variety of orbital maneuvering and payload injection and retrieval mission applications. The RST will be capable of both manned and unmanned autonomous operation. When used as an unmanned Earth-based stage for payload injection missions the RST will be carried to a circular low Earth orbit (LEO) inside the cargo bay of the space shuttle orbiter. It will leave the orbiter, deliver its payload to the required injection conditions, then return to the waiting orbiter and reenter the cargo bay for the return flight to Earth. In the unmanned space-based mode the RST will also begin and end each mission in LEO, possibly at an orbiting propellant depot or some other facility. This paper presents optimum round trip trajectories for payload injection missions at energy levels above Earth escape. The trajectories are applicable to both Earth-based and space-based modes of operation.

The ideal performance capability of an RST for round trip missions to energy levels above Earth escape can be easily calculated if all burns

are assumed to be impulsive (of zero time duration). All real vehicles, however, are limited to finite thrust levels. The burn time required to reach the specified vis-viva injection energy (C_3) is a function of the ignition thrust-to-weight ratio (α). When the vehicle reaches the specified energy level, the payload must be separated from the RST, the RST must be turned around in preparation for the return flight to LEO, and any necessary separation distance between the RST and payload (to prevent damage to the spacecraft by RST exhaust impingement) must be accumulated. The duration of the payload separation and vehicle turn around phase (which is the time spent at the specified C_3 by the RST) is referred to as the turn-around time (TAT) in this paper. During the TAT coast phase the RST is on a hyperbolic trajectory and its altitude is increasing. Losses incurred during the burn phase which follows the TAT coast are a function of the altitude at which the burn occurs and therefore depend on the TAT. In the ideal case, all burn phases are assumed to take place at the LEO altitude. In the real case the RST leaves the circular LEO at the instant the first burn begins and reenters the same LEO at the instant of final burnout. The elapsed time spent out of the LEO is called the total trip time (TTT) in this paper. The total ΔV requirements and the performance capability are functions of the TTT. The purpose of this study is to determine optimum round trip trajectories with these real vehicle constraints included.

The maximum principle of the calculus of variations is used to formulate the mathematical problem and determine the costate equations. The state and costate equations are numerically integrated to determine the vehicle motion, the location and duration of burn phases and the final conditions of the two point boundary value problem associated with the optimum solution. Partial derivatives of the boundary value problem final conditions with respect to initial conditions are obtained by finite difference methods. The boundary value problem is solved by use of a simple Newton-Raphson linear iteration scheme.

In order to demonstrate the effect of the various vehicle constraints, some parametric results are presented. Normalized payload mass loss (compared to the ideal calculated capability) is shown as a function of α for discrete positive values of C_3. The α ranges from 0.3 to 10.0. Results are repeated for TAT's of 3 and 6 minutes and for engine specific impulse (I) values of 444 and 460 seconds. The values of I were chosen to represent current and feasible liquid hydrogen-liquid oxygen engine technology, respectively. The effects of TAT's up to 10 minutes and TTT's between 6 and 1000 hours are demonstrated for representative cases. A TTT of 24 hours is chosen as a baseline value for the parametric results. Propellant mass fraction (MF) values of 0.84, 0.87, and 0.90 are included. The initial LEO altitude is assumed to be 185 kilometers. Effects of the Earth's oblateness are omitted for convenience.

Trajectory Characteristics

In calculating the ideal performance capability, all burns are assumed to occur at the LEO altitude. One might expect that for real vehicle trajectories the RST would burn continuously from the LEO to the specified C_3, coast for the required TAT, and then burn continuously until it reentered the original LEO. For C_3 values above Earth escape and reasonable values of α and TAT, optimum trajectories to the specified C_3 result in very high altitudes at the end of the TAT coast. Continuous thrust trajectories from a high altitude back to LEO require very high ΔV's. The altitude following the TAT can be reduced by compromising the first burn thrust profile to "hold the trajectory in" but this approach is also costly from a ΔV standpoint. Determination of the optimum round trip trajectory must admit the possibility of alternate powered and coast phases during both the outbound and inbound legs.

For the parameter ranges considered in this study the optimum round trip trajectories were found to consist of:

1) A continuous main burn from the original LEO to the specified C_3.

2) The imposed TAT coast phase.

3) A retro burn which reduces the energy of the RST to a value below Earth escape after which the RST is in an elliptical transfer orbit.

4) A coast to near apogee of the transfer orbit.

5) A short apogee burn phase which adjusts the perigee of the transfer orbit to approximately the LEO altitude.

6) A coast to near perigee of the adjusted transfer orbit.

7) A final circularization burn which returns the RST to the original LEO.

These phases are depicted graphically in sketch a.

Analysis

The problem to be solved is to maximize the payload mass which can be delivered to a specified energy level above Earth escape by a stage of known characteristics (I, α, and MF) which starts in a specified LEO and returns to the same orbit after releasing the payload. For a vehicle with infinite thrust and zero turn-around time capability, the ratio of payload mass to initial mass (including payload) can be calculated as

$$\frac{m_{pl}}{m_0} = \frac{\delta(R^2 - 1) - 1}{R[\delta(R - 1) - 1]} \qquad (1)$$

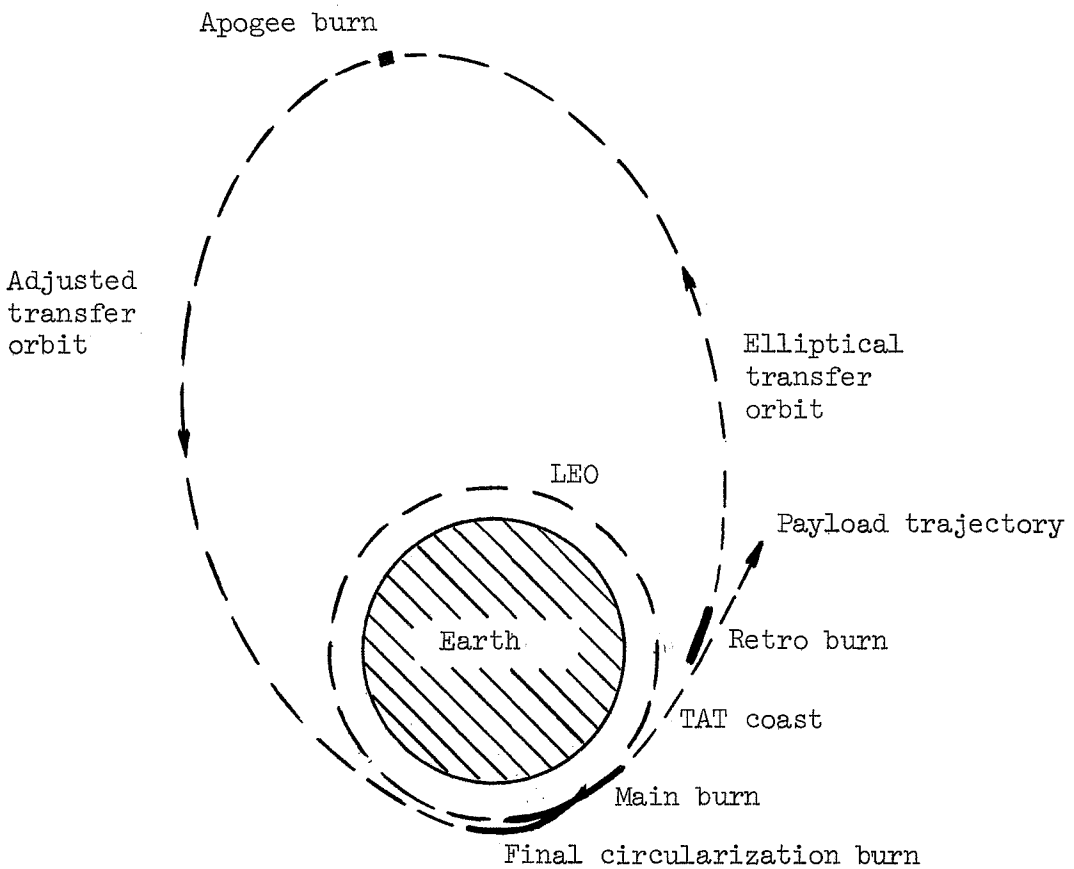

Sketch a. Optimum trajectory profile.

where δ is the ratio of stage jettison mass to propellant mass and can be written in terms of MF as

$$\delta = \frac{1 - MF}{MF}$$

and R is the ratio of ignition mass to burnout mass for an ideal impulsive propulsion maneuver which imparts the ΔV required to reach the specified energy level. The value of R is calculated as

$$R = e^{\Delta V/C}$$

All symbols are defined in appendix A.

The variational maximum principle is used to formulate and solve the problem for the case of real vehicles with finite thrust levels and non-

zero TAT capability. The two point boundary value problem associated with the optimum solution consists of four final conditions which must be satisfied and an equal number of initial conditions to be chosen. It was found that because of the long flight times involved, minor adjustments in the initial conditions cause large variations in the resulting final conditions. This extreme sensitivity makes the boundary value problem difficult to solve by simple techniques. A number of solutions were obtained and the trajectories examined. They consist of the seven distinct phases described in the Trajectory Characteristics section above.

Because of the sensitivity of the boundary value problem and based on the observed characteristics of the optimum trajectories, an alternate, approximate technique was developed. The method is based on the assumption that the apogee burn occurs precisely at apogee, is impulsive and tangential, and adjusts the transfer orbit perigee altitude to coincide with the original LEO. The final circularization burn is also tangential and impulsive. The gravity losses which would be associated with finite thrust final burns were determined by independently integrated calculus of variations trajectories and added to the impulsive ΔV requirement for the final burn. Details of the approximate method analysis are presented in appendix B. The three final conditions of the boundary value problem associated with the approximate solution are all evaluated at the end of the retro burn. The long transfer orbit coast phases, the apogee burn, and the final circularization burn are not numerically integrated. This boundary value problem is considerably less sensitive than the exact one and solutions were obtained more easily.

For all cases in which a comparison was made, the payload capability determined by the exact and approximate methods differed by no more than two one-hundredths of one percent of the initial starting mass. The actual comparison values are shown in table I.

The calculated apogee ΔV for all trajectories generated by the approximate method was less than 50 meters per second. The ΔV requirement for the final circularization burn is a function of the energy of the transfer orbit. For a TTT of 24 hours the transfer orbit vis-viva energy is about -9.45 km^2/sec^2. The final circularization ΔV for a TTT of 24 hours varies from 2.79 to 2.81 km/sec. The gravity losses added to the circularization ΔV requirement are a function of the energy of the transfer ellipse and the vehicle thrust-to-weight ratio at the start of the final maneuver. The losses do not exceed 4 meters per second for any of the trajectories considered in this study.

Although not explicitly presented, the propellant requirements for a particular case can be easily determined. The initial mass (m_0) includes the payload mass (m_{pl}), propellant mass (m_{pr}), and stage jettison mass (m_j). Since the propellant mass fraction (MF) is specified, the propellant mass can be calculated as

$$\frac{m_{pr}}{m_0} = MF\left(1 - \frac{m_{pl}}{m_0}\right) \tag{2}$$

Results and Discussion

The ideal impulsive performance capability of a reusable stage (as calculated from eq. (1)) is shown in Figure 1. Normalized payload mass (m_{pl}/m_0) capability is shown as a function of the vis-viva energy to which it is delivered. The performance of Figure 1 applies to a RST which has infinite thrust and can fly a zero TAT trajectory. Since the payload losses are usually small compared to the ideal capability, subsequent results in this paper are in terms of normalized payload mass loss ($\Delta m_{pl}/m_0$) which allows the actual capability to be determined more accurately.

Procedure for Using Results

The results to be presented are applicable to a variety of situations. When the initial mass (m_0), the mission C_3 and the RST characteristics (I, α, and MF) are known, the results can be applied directly. The initial mass is known when the RST is Earth-based and the mission is to be accomplished with a single launch of a space shuttle of known capability, for example. When the initial mass is not specified and some other criteria is established (e.g., specified RST propellant capacity, specified payload mass requirement, etc.). The results can still be used, but a simple iteration is necessary. The following steps are required:

(1) Estimate m_0.

(2) Calculate the ideal m_{pl}/m_0 from equation (1).

(3) Determine the loss ($\Delta m_{pl}/m_0$) from the appropriate curve.

(4) Calculate the actual capability as $m_{pl}/m_0 - \Delta m_{pl}/m_0$.

(5) Compute the propellant mass required from equation (2) and any parameters involved in the established criteria.

(6) If the desired criteria is satisfied terminate the iteration. Otherwise adjust m_0 and return to step (2).

Effect of TAT and TTT

The effect of vehicle TAT on normalized payload mass loss is shown for a representative case in Figure 2. When the TAT is zero the payload loss is minimized but is nonzero because of the finite α. As TAT increases the payload loss increases so the actual performance capability

decreases. At a fixed TAT the losses are greater for the lower MF values. This is true because of the higher final jettison mass and lower payload mass associated with the lower MF which results in a lower average thrust to mass ratio (and higher losses) during the retro and final circularization burns.

The RST is at an energy level above Earth escape during the TAT coast and its altitude is increasing. Since the energy remains constant the velocity is decreasing. The reduction in energy which must be accomplished during the retro burn following the TAT coast is more efficiently achieved at lower altitudes and higher velocities. It is obvious then, both from a logical approach and from Figure 2, that the TAT should be as short as possible. During the TAT coast the RST must be turned around in preparation for the retro burn. The required orientation is such that the exhaust gases are directed almost directly toward the separated spacecraft. To prevent damage to the spacecraft by RST exhaust impingement some minimum separation distance must be accumulated before the RST engine is ignited for the retro maneuver. A detailed analysis to determine the minimum necessary separation distance was not undertaken as part of this study. TAT's of 3 and 6 minutes are used as baseline values. The performance advantage of short TAT's must be compared to the operational difficulty of separating the payload, turning the vehicle around and accumulating the necessary separation distance in a short time.

The necessary decrease in the energy of the RST (from the payload injection level to the LEO value) is accomplished primarily during the retro burn following the TAT coast and during the final circularization burn. For all reasonable values of α and TAT, the altitude is lower and the velocity is higher at the start of the final burn than at the end of the retro burn. Therefore, the energy decrease is more efficiently accomplished during the final burn than during the retro burn, and the retro burn should be kept as short as possible. The minimum possible retro burn for a reusable vehicle reduces the RST energy to exactly zero (Earth escape). The resulting TTT is infinite.

The effect of finite TTT's between 6 and 1000 hours is shown in Figure 3 for representative values of the other parameters. As TTT decreases from its optimum (but impractical) value of infinity the payload loss increases. The performance advantage of long TTT's must be compromised because of the obvious operational advantages of much shorter TTT's. For an Earth-based, single shuttle launch mission, the orbiter must wait for the RST in the LEO for the entire TTT. A phasing problem is involved since the RST must rendezvous and dock with the orbiter after returning to LEO. Proper phasing can be achieved by making slight (less than 1 hour) adjustments to the TTT. As shown in Figure 3, a change of this magnitude has very little effect on the performance capability at the longer TTT's. For simplicity the rendezvous requirement is ignored in this study. If very short TTT's are desired, the effect of the rendezvous requirement would have to be included. A TTT of 24 hours is chosen as a baseline value for demonstrating the effects of other parameters in this study.

General Results

The normalized payload mass loss $\Delta m_{pl}/m_0$ is presented as a function of α for I = 444 and 460 seconds in Figures 4 and 5, respectively. The TTT is 24 hours in both cases. Part (a) of both figures is for MF = 0.90 and TAT = 3 minutes. Part (b) is for the same MF and a TAT of 6 minutes. The (c) and (d) parts of both figures correspond to a MF of 0.87 and TAT's of 3 and 6 minutes, respectively. Parts (e) and (f) repeat the pattern with MF = 0.84. Attainable, positive values of C_3 are included on each of the plots. Curves that end in the middle of a plot stop at the point where the payload capability is zero.

All parts of Figures 4 and 5 illustrate the same characteristics. The payload losses increase as α decreases. The increase is very rapid for α values below about 2.0 at the highest energy levels and for α values below about 1.0 at all energy levels. This behavior is significant since for expendable vehicle trajectories to energy levels above Earth escape, substantially lower thrust-to-weight ratios can be tolerated without large payload penalties. Further examination of Figures 4 and 5 indicates that for any specific value of α the payload loss increases with increasing C_3, is higher for TAT = 6 minutes than for TAT = 3 minutes, and is higher for I = 444 than for I = 460 seconds. At constant values of α, C_3, I, TAT, and TTT, the payload loss increases with decreasing MF.

Trajectory Characteristics

The time (t) history of various trajectory parameters is presented in Figure 6 for a representative case. Values of α of 10.0, 0.5, and 0.3 are included. The variation of altitude (Z), velocity (v), vis-viva energy (C_3), flight path angle (θ), thrust attitude (ψ), and inertial travel angle (ϕ) with time is shown in parts (a) through (f), respectively. The angles θ, ψ, and ϕ are defined graphically in Figure 7. The solid line segments in Figure 6 represent the main and retro burn segments of the trajectory and the dashed portion applies to the TAT coast. Parameter histories during the transfer orbit coast phase, the apogee burn phase, and the final circularization burn are not shown. If desired, they can be calculated from the values at the end of the retro burn and the description of the approximate trajectory.

At t = 0 the RST is in the LEO. The altitude, velocity, and energy values are those of the LEO and are the same for any value of α. The flight path angle is zero because the orbit is circular and the travel angle is zero by definition. The thrust angle at t = 0 is the initial value determined by solving the two point boundary value problem. It is negative and a function of α. As a result, both θ and z decrease slightly at first. The angle θ becomes negative and z becomes less than the original LEO altitude of 185 kilometers. As time proceeds, v increases; C_3, ψ, and eventually θ and z also increase. At the end of the main burn C_3 is equal to the specified 15 km^2/sec^2.

The altitude is greater than 185 kilometers and greater for lower α values. The velocity at the end of the main burn is that required by the condition $C_3 = 15$ km^2/sec^2 at the burnout altitude. The angle ψ is slightly less than θ. For optimum one-way (expendable vehicle) trajectories, ψ is equal to θ at the specified energy level. For optimum round trip trajectories the first burn is compromised somewhat in order that losses incurred during the retro burn are reduced.

During the TAT coast phase, z continues to increase as mentioned earlier, v decreases, and C_3 remains constant. At the end of the TAT coast, the calculated value of ψ changes instantaneously to the optimum value required for the retro burn. Examination of ψ and θ at the start of the retro indicates that the thrust and velocity vectors are nearly antiparallel.

During the retro burn v decreases until C_3 is equal to the -9.45 km^2/sec^2 required for the elliptical transfer orbit when TTT = 24 hours. The thrust and velocity vectors remain nearly antiparallel during the retro burn.

Conclusions

Optimum round trip trajectories for payload injection missions above Earth escape energy are determined by solving the appropriate two point boundary value problem. The four final conditions of the boundary value problem are extremely sensitive to small changes in the initial conditions. Although difficult, the boundary value problem can be solved using linear finite difference Newton-Raphson iteration techniques.

The optimum trajectories consist of a continuous main burn from the initial low Earth orbit to the specified energy level, a coast phase of specified duration during which the payload is separated and the vehicle turned nearly 180 degrees, a retro burn which reduces the energy to a value below Earth escape which is primarily a function of the desired total trip time, a coast to near apogee of the elliptical transfer orbit, a short apogee burn which adjusts the perigee of the transfer orbit to a value close to the original low Earth orbit altitude, a coast to near perigee of the adjusted transfer orbit, and a final circularization burn which returns the vehicle to the initial low Earth orbit.

Essentially optimum approximate trajectories can be obtained easily by using the same simple iteration technique to solve an alternate two point boundary value problem. The approximate trajectories differ from the optimum ones in that the apogee and perigee burns are assumed to be impulsive and tangential and occur exactly at apogee and perigee. The magnitude of the apogee burn is calculated to adjust the perigee altitude of the transfer orbit to exactly the original low Earth orbit value.

For maximum payload to a specified energy level above Earth escape, the turn-around coast phase should be as short as possible and the total

trip time as long as is operationally practical. The vehicle thrust level has a strong effect on its performance capability. For the same ignition thrust-to-weight ratio the losses are significantly higher for a round trip trajectory than for a one-way trajectory to the same energy level.

APPENDIX A

SYMBOLS

C_3	vis-viva energy, km^2/sec^2
c	jet velocity, km/sec
E	energy, km^2/sec^2
e	eccentricity, N.D.
$\hat{f}$	thrust direction, N.D.
G	universal gravitational constant, km^3/sec^2-kg
H	Hamiltonian, kg/sec
h	angular momentum, km^2/sec
I	specific impulse, sec
J	jump discontinuity in $(\rho - H)$, kg/sec
m	mass, kg
Δm_{pl}	payload mass loss, kg
R	mass ratio, m_0/m_f, N.D.
r	radius, km
t	time, sec
u	throttle control, N.D.
ΔV	characteristic velocity increment, km/sec
v	velocity, km/sec
x	state variable used in (D11)
Z	altitude, km
α	ratio of thrust to equivalent vehicle equatorial surface weight at ignition, N.D.
β	maximum mass flow rate, kg/sec
γ	yaw attitude, deg

δ ratio of stage jettison mass to propellant mass, N.D.

ε jump factor, $kg\text{-}sec^2/km^2$

η jump factor, $kg\text{-}sec^2/km^2$

θ flight path angle, deg

κ power-coast switching function, N.D.

λ costate variable, kg-sec/km

μ costate variable, kg/km

ρ costate variable, kg/sec

σ costate variable, N.D.

τ state variable equivalent to time, sec

ϕ travel angle, deg

ψ pitch attitude, deg

Subscripts:

a apogee

e Earth

f final

j jettison

max overall maximum

p perigee

pl payload

pr propellant

r retro burnout

0 initial

1 start of TAT coast

2 end of TAT coast

Superscripts:

$\vec{}$	vector
$\dot{}$	time derivative
$\hat{}$	unit vector
+	after event
-	before event

Abbreviations:

LEO	low Earth orbit (circular at 185 km altitude)
MF	propellant mass fraction (ratio of propellant mass to stage mass)
RST	reusable space tug
TAT	turn-around time (duration of payload separation and vehicle turn-around coast phase)
TTT	total trip time

APPENDIX B

MATHEMATICAL FORMULATION OF APPROXIMATE SOLUTION

Because of the sensitivity of final to initial boundary value conditions for rigorously optimized round-trip space-tug trajectories, an approximate technique based on the observed characteristics of the optimum trajectories was developed. The approximate method was highly successful from a convergence standpoint, and gave payload masses which differed very little from the optimum values.

The numerically integrated portion of the approximate trajectory consists of the main burn, imposed TAT coast, and retro burn. The retro burn is terminated when the coast time to perigee on the resulting elliptical transfer orbit is equal to the specified TTT, less the elapsed time to that point. The perigee altitude is not specified, and in general differs from the specified LEO altitude. This difference is removed by a small impulse which is assumed to take place precisely at apogee, with a tangential thrust direction. The apogee burn modifies the orbital period only slightly, and this difference is neglected in the mathematical formulation. The final burn is also assumed to be impulsive, utilizes tangential thrusting, and takes place precisely at perigee. Since the magnitude of the final impulse depends only on the trip time, this burn is not included in the variational problem. However, the calculated perigee impulse (including an appropriate loss due to finite thrust level) is included in the calculation of final mass. The magnitude of the apogee impulse depends on the perigee at retro burnout, and its effect is included in the variational problem, as well as in the calculation of final mass.

The variational problem to be solved is to maximize the payload mass which can be delivered to a fixed energy level by a fixed mass fraction, reusable space tug. After releasing the payload, the tug must satisfy certain final conditions. A fixed duration TAT coast phase is imposed. The available controls are the thrust direction and engine thrust level (on or off). The mathematical problem is formulated by using the variational maximum principle (ref. 1), with equations of motion as follows:

$$\dot{\bar{v}} = -\frac{Gm_e}{r^3}\bar{r} + \frac{c\beta u}{m}\hat{f} \qquad \text{(a)}$$

$$\dot{\bar{r}} = \bar{v} \qquad \text{(b)} \qquad \text{(B1)}$$

$$\dot{m} = -\beta u \qquad \text{(c)}$$

$$\dot{\tau} = 1 \qquad \text{(d)}$$

where $\beta = \beta(\tau)$ is the maximum allowable flow rate (engine operating at full thrust) and τ (equivalent to time) is introduced to make the system autonomous. All symbols are defined in appendix A. The controls are the throttle u and thrust direction $\hat{f}$, subject to $|\hat{f}| = 1$ and $u = 0$

(engine off) or 1 (engine on). The variational Hamiltonian is

$$H = \bar{\lambda} \cdot \left[-\frac{Gm_e}{r^3} \bar{r} + \frac{c\beta u}{m} \hat{f} \right] + \bar{\mu} \cdot \bar{v} - \sigma\beta u + \rho \tag{B2}$$

where ρ is the multiplier for τ. The costate equations are

$$\dot{\bar{\lambda}} = -\bar{\mu} \tag{a}$$

$$\dot{\bar{\mu}} = \frac{Gm_e}{r^3} \bar{\lambda} - \frac{3Gm_e}{r^5} (\bar{\lambda} \cdot \bar{r})\bar{r} \tag{b}$$

(B3)

$$\dot{\sigma} = \frac{c\beta u}{m^2} \bar{\lambda} \cdot \hat{f} \tag{c}$$

$$\dot{\rho} = -\left(\frac{c}{m} \bar{\lambda} \cdot \hat{f} - \sigma\right) u \frac{d\beta}{dt} \tag{d}$$

The optimal controls are obtained by maximizing H, which results in

$$\hat{f} = \hat{\lambda} \tag{B4}$$

and

$$u = \begin{cases} 1, & \kappa > 0 \\ 0, & \kappa < 0 \end{cases} \tag{B5}$$

where κ is defined as

$$\kappa = \frac{c}{m} \lambda - \sigma \tag{B6}$$

It should be noted that H is a constant of the motion and, if β is constant, ρ is also constant.

Boundary Conditions

Define:

t_0 initial time

t_1 time at which energy level for payload jettison is achieved; start TAT coast

t_2 end TAT coast and jettison payload (Actually, the payload would be jettisoned as soon after t_1 as possible. Since there is no propulsion between t_1 and t_2, all payload jettison times between t_1 and t_2 are mathematically equivalent.)

t_r completion of retro burn

t_f final time

then $\beta(t)$ is given by

$$\beta = \begin{cases} \beta_{max}, & t_0 \le t \le t_1 \quad \text{and} \quad t_2 \le t \le t_r \\ 0, & t_1 < t < t_2 \end{cases}$$

Any one of the above time points may be considered fixed, since the time reference is arbitrary. It is convenient to consider t_1 fixed, which also fixes t_2. Also, the reference value of τ is established by choosing $\tau(t_0) = t_0$. The initial orbit is completely specified, as are the initial mass and payload energy. Since the mass fraction is specified, the mass at retro burnout is required to be

$$m_r = e^{(\Delta V_a + \Delta V_p)/c} (1 - MF)(m_0 - m_{pl}) \tag{B7}$$

where ΔV_a is the velocity increment required at apogee to adjust the perigee altitude to 185 km.

Transversality Equation

The transversality equation for this problem may be written

$$\begin{aligned} &(\bar{\lambda} \cdot d\bar{v} + \bar{\mu} \cdot d\bar{r} + \sigma\, dm + \rho\, d\tau - H\, dt)_{t_r} \\ &\quad - (\bar{\lambda} \cdot d\bar{v} + \bar{\mu} \cdot d\bar{r} + \sigma\, dm + \rho\, d\tau - H\, dt)_{t_2^+} \\ &\quad + (\bar{\lambda} \cdot d\bar{v} + \bar{\mu} \cdot d\bar{r} + \sigma\, dm + \rho\, d\tau - H\, dt)_{t_2^-} \\ &\quad - (\bar{\lambda} \cdot d\bar{v} + \bar{\mu} \cdot d\bar{r} + \sigma\, dm + \rho\, d\tau - H\, dt)_{t_1^+} \\ &\quad + (\bar{\lambda} \cdot d\bar{v} + \bar{\mu} \cdot d\bar{r} + \sigma\, dm + \rho\, d\tau - H\, dt)_{t_1^-} \\ &\quad - (\bar{\lambda} \cdot d\bar{v} + \bar{\mu} \cdot d\bar{r} + \sigma\, dm + \rho\, d\tau - H\, dt)_{t_0} \\ &\quad - dm_{pl} = 0 \end{aligned} \tag{B8}$$

Substituting the fixed boundary conditions into (B8) and setting the coefficients of the remaining (free) variations equal to zero results in

$$\sigma_2^+ - \sigma_2^- = \sigma_1^- - \sigma_1^+ \qquad \text{(a)}$$

$$(\rho - H)_r = (\rho - H)_0 \qquad \text{(b)}$$

$$(\rho - H)_0 = 0 \qquad \text{(c)}$$

$$\sigma_r(MF - 1)e^{(\Delta V_a + \Delta V_p)/c} + \sigma_2^+ = 1 \qquad \text{(d)}$$

$$\left(\bar{\lambda} + \frac{m\sigma}{c}\frac{\partial \Delta V_a}{\partial \bar{V}} - \eta\bar{v}\right)_{t_r} = \bar{0} \qquad \text{(e)} \qquad \text{(B9)}$$

$$\left(\bar{\mu} + \frac{m\sigma}{c}\frac{\partial \Delta V_a}{\partial \bar{r}} - \eta\frac{Gm_e}{r^3}\bar{r}\right)_{t_r} = \bar{0} \qquad \text{(f)}$$

$$\bar{\lambda}_2^+ = \bar{\lambda}_2^- + \varepsilon\bar{V}_2 \qquad \text{(g)}$$

$$\bar{\mu}_2^+ = \bar{\mu}_2^- + \varepsilon\frac{Gm_e}{r_2^3}\bar{r}_2 \qquad \text{(h)}$$

The multiplier η in (B9d) and (B9e) results from the specified energy at retro burnout. The partial derivatives $\partial\Delta V_a/\partial\bar{V}$ and $\partial\Delta V_a/\partial\bar{r}$ will be determined later. Also, the multipliers $\bar{\lambda}$ and $\bar{\mu}$ are discontinuous at t_2 (with jump factor ε), since energy is specified at that time (see ref. 1).

In addition to (B9), the following specified boundary conditions must be satisfied:

$$E_1 \qquad \text{(a)}$$

$$E_r \qquad \text{(b)} \qquad \text{(B10)}$$

$$\frac{m_0 - m_f - m_{pl}}{m_0 - m_{pl}} \qquad \text{(c)}$$

Equation (B10c), equivalent to (B7), is the calculated value of propellant mass fraction, assuming that the total mass returned to the LEO is stage jettison mass; the calculated mass fraction must be equal to the

specified mass fraction.

A number of initial conditions are available in order to allow (B9) and (B10) to be satisfied. These are:

ψ_0	(a)	σ_0	(g)
$\dot{\psi}_0$	(b)	t_0	(h)
γ_0	(c)	ε	(i)
$\dot{\gamma}_0$	(d)	m_{pl}	(j)
λ_0	(e)	t_r	(k)
$\dot{\lambda}_0$	(f)		

(B11)

where initial values of the multipliers $\bar{\lambda}$ and $\bar{\mu}$ are expressed in terms of the initial magnitude of $\bar{\lambda}$, pitch and yaw attitudes, and the corresponding rates (B11a through f) as in reference 2. The angles ψ and γ are defined in Figure 8.

The main burn may be terminated when E_1 (B10a) is satisfied, which also determines t_0 (B11h). Similarly, the retro burn is terminated when E_r (B10b) is satisfied, and this procedure determines t_r (B11k). Also, σ_0 (B11g) may be calculated from (B2) in order to satisfy (B9c).

Consider next the procedure for satisfying (B9b). Since $(\rho - H)$ is constant when β is constant, (B9b) may be written

$$(\rho - H)_r - (\rho - H)_0 = (\rho - H)_{t_1^-} - (\rho - H)_{t_2^+} = 0 \tag{B12}$$

Also,

$$(\rho - H)_{t_1^+} = (\rho - H)_{t_1^-} + J_1$$

$$(\rho - H)_{t_2^+} = (\rho - H)_{t_2^-} + J_2$$

where J_1 and J_2 are the jump discontinuities in $(\rho - H)$ at t_1 and t_2, respectively. Also,

$$(\rho - H)_{t_1^+} = (\rho - H)_{t_2^-}$$

Therefore, (B12) becomes

$$(\rho - H)_{t_1^-} - (\rho - H)_{t_2^+} = (\rho - H)_{t_1^+} - J_1 - (\rho - H)_{t_2^-} - J_2 = 0$$

or

$$J_1 + J_2 = 0$$

The jumps, J_1 and J_2, can be evaluated by using (B2) and recalling that $\beta_{t_1^+} = \beta_{t_2^-} = 0$:

$$J_1 = -\left\{\bar{\lambda} \cdot \left[-\frac{Gm_e}{r^3}\bar{r} + \frac{c\beta u}{m}\hat{f}\right] + \bar{\mu} \cdot \bar{V} - \sigma\beta u\right\}_{t_1^+}$$

$$+\left\{\bar{\lambda} \cdot \left[-\frac{Gm_e}{r^3}\bar{r} + \frac{c\beta u}{m}\hat{f}\right] + \bar{\mu} \cdot \bar{V} - \sigma\beta u\right\}_{t_1^-}$$

$$= \left(\frac{c\beta u\lambda}{m} - \sigma\beta u\right)_{t_1^-} = (\kappa\beta_{max}u)_{t_1^-} \qquad \text{(B13a)}$$

$$J_2 = -\left\{\bar{\lambda} \cdot \left[-\frac{Gm_e}{r^3}\bar{r} + \frac{c\beta u}{m}\hat{f}\right] + \bar{\mu} \cdot \bar{V} - \sigma\beta u\right\}_{t_2^+}$$

$$+\left\{\bar{\lambda} \cdot \left[-\frac{Gm_e}{r^3}\bar{r} + \frac{c\beta u}{m}\hat{f}\right] + \bar{\mu} \cdot \bar{V} - \sigma\beta u\right\}_{t_2^-}$$

$$= -\varepsilon\bar{V}_2 \cdot \left(-\frac{Gm_e}{r_2^3}\bar{r}_2\right) - \varepsilon\frac{Gm_e}{r_2^3}\bar{r}_2 \cdot \bar{V}_2 - \left(\frac{c\beta u}{m}\lambda - \sigma\beta u\right)_{t_2^+}$$

$$= -(\kappa\beta_{max}u)_{t_2^+} \qquad \text{(B13b)}$$

Therefore,

$$J_1 + J_2 = \beta_{max}\left[\left(\frac{c}{m}\lambda - \sigma\right)u_{t_1^-} - \left(\frac{c}{m}\lambda - \sigma\right)u_{t_2^+}\right] \qquad \text{(B14)}$$

Now from (B9a),

$$\sigma_2^+ - \sigma_1^- = \sigma_2^- - \sigma_1^+ = 0 \qquad \text{(B15)}$$

since σ is constant between t_1 and t_2. Also, $u_{t_1^-} = 1$ since thrusting is required to reach the payload separation energy, E_1. If $u_{t_2^+} = 0$,

(B14) cannot be made equal to zero (except for the special case $\kappa_{t_1^-} = 0$). Therefore, it must be assumed that $u_{t_2^+} = 1$. Now using (B15) in (B14) results in

$$J_1 + J_2 = c\beta_{max}\left[\left(\frac{\lambda}{m}\right)_{t_1^-} - \left(\frac{\lambda}{m}\right)_{t_2^+}\right] = 0 \tag{B16}$$

The value of ε may be chosen to satisfy (B16); the procedure is as follows:

$$\bar{\lambda}_2^+ = \bar{\lambda}_2^- + \varepsilon\bar{V}_2$$

$$\lambda_2^+ = \sqrt{\lambda_2^{-2} + \varepsilon^2 V_2^2 + 2\varepsilon\bar{\lambda}_2^- \cdot \bar{V}_2} = \left(\frac{m_2^+}{m_1^-}\right)\lambda_1$$

Solving for ε results in

$$\varepsilon = -\frac{\bar{\lambda}_2^- \cdot \bar{V}_2 \pm \sqrt{(\bar{\lambda}_2^- \cdot \bar{V}_2)^2 - \lambda_2^2 V_2^2 + \left(\frac{m_2^+}{m_1^-}\right)^2 \lambda_1^2 V_2^2}}{V_2^2}$$

which may be written as

$$\varepsilon = \frac{1}{V_2}\left\{-\bar{\lambda}_2^- \cdot \hat{V}_2 \pm \sqrt{\left(\frac{m_2^+}{m_1^-}\right)^2 \lambda_1^2 - |\bar{\lambda}_2^- \times \hat{V}_2|^2}\right\} \tag{B17}$$

The sign choice may be made by applying physical reasoning to the problem. It is expected that the thrust should be directed approximately parallel to the velocity vector when it is desired to increase velocity (up to t_2^-) and approximately antiparallel to the velocity vector when it is desired to decrease velocity (from t_2^+ to t_r). Then

$$\bar{\lambda}_2^- \sim \lambda_2^-\hat{V}_2$$

$$\bar{\lambda}_2^+ \sim -\lambda_2^+\hat{V}_2$$

$$\varepsilon \sim \frac{1}{V_2}\left[-\lambda_2 \pm \left(\frac{m_2^+}{m_1^-}\right)\lambda_1\right]$$

But

$$\bar{\lambda}_2^+ = \bar{\lambda}_2^- + \varepsilon \bar{V}_2$$

$$-\lambda_2^- \hat{V}_2 + \frac{1}{V_2}\left[-\bar{\lambda}_2^- \pm \left(\frac{m_2^+}{m_2^-}\right)\bar{V}_2\right] = \pm\left(\frac{m_2^+}{m_1^-}\right)\lambda_1 \hat{V}_2$$

Therefore, the minus sign should be chosen:

$$\varepsilon = \frac{1}{V_2}\left\{-\bar{\lambda}_2 \cdot \hat{V}_2 - \sqrt{\left(\frac{m_2^+}{m_1^-}\right)^2 \lambda_1^2 - \left|\bar{\lambda}_2^- \times \hat{V}_2\right|^2}\right\}$$

This procedure for calculating ε eliminates (B11i) and (B9b) from the boundary value problem. Also, the initial value λ_0 (B11e) may be chosen to satisfy (B9d) without affecting the trajectory, since the costate equations are homogeneous in the multipliers.

Finally, it remains to manipulate (B9d) and (B9e) into a more suitable form. The value of η may be chosen to equate the magnitude of the left and right sides of (B9a), i.e.,

$$\lambda = \pm\left|\bar{\lambda} + \frac{m\sigma}{c}\frac{\partial \Delta V_a}{\partial \bar{V}}\right| \Big/ V \qquad \text{(B18)}$$

The sign choice in (B18) is made as follows. If the apogee impulse were not a function of the retro burnout conditions, (B18) would reduce to

$$\eta = \pm\frac{\lambda}{V}$$

and (B9a) would give

$$\bar{\lambda} = \lambda \hat{V} \qquad \text{(a)}$$

and (B19)

$$\hat{f} = \pm\hat{V} \qquad \text{(b)}$$

Now since the retro burn removes energy, it is clear that the minus sign should be chosen in (B19), hence also in (B18). Therefore, η becomes

$$\eta = -\left|\bar{\lambda} + \frac{m\sigma}{c}\frac{\partial \Delta V_a}{\partial \bar{V}}\right| \Big/ V \qquad \text{(B20)}$$

Since η has been selected to satisfy the magnitude of (B9e), equations (B9e) and (B9f) have been reduced to five equations. Three of these may be expressed as

$$\bar{\lambda} \times \bar{V} + \bar{\mu} \times \bar{r} = \bar{0} \tag{B21}$$

which may be verified by taking the cross products of (B9e) with $\bar{V}$ and (B9f) with $\bar{r}$, adding, and noting as in appendix B of reference 3 that

$$\frac{\partial \Delta V_a}{\partial \bar{V}} \times \bar{V} + \frac{\partial \Delta V_a}{\partial \bar{r}} \times \bar{r} = \bar{0}$$

Equations (B21) are constants of the motion which are not affected by the jump in $\bar{\lambda}$ and $\bar{\mu}$ at t_2 (eqs. (B9g) and (B9h); see ref. 3), and are used to calculate γ_0, $\dot{\gamma}_0$, and λ_0. Specifically, the result is

$$\begin{aligned} \gamma_0 &= 0 \\ \dot{\gamma}_0 &= 0 \\ \lambda_0 &= \left[\frac{\lambda(\hat{\lambda} \times \bar{V} - \dot{\hat{\lambda}} \times \bar{r}) \cdot \hat{h}}{(\hat{\lambda} \times \bar{r}) \cdot \hat{h}} \right]_{t_0} \end{aligned} \tag{B22}$$

The remaining two equations in (B9) can be expressed as

$$\begin{aligned} &\left(\bar{\lambda} + \frac{m\sigma}{c} \frac{\partial \Delta V_a}{\partial \bar{V}} \right) \cdot \bar{V} = \eta V^2 \qquad \text{(a)} \\ &\left(\bar{\mu} + \frac{m\sigma}{c} \frac{\partial \Delta V_a}{\partial \bar{r}} \right) \cdot \bar{r} = \eta \frac{Gm_e}{r} \qquad \text{(b)} \end{aligned} \tag{B23}$$

The initial and final conditions in the two point boundary value problem are as follows.

Initial conditions	Final conditions
ψ_0	eq. (B10c)
$\dot{\psi}_0$	eq. (B23a)
m_{pl}	eq. (B23b)

Calculation of Apogee Impulse and Partial Derivatives

The ΔV_a required to raise the perigee altitude of the transfer orbit to the final LEO altitude is given by

$$\Delta V_a = \sqrt{\frac{2\mu r_f}{r_a(r_a + r_f)}} - \sqrt{\frac{2\mu r_p}{r_a(r_a + r_p)}} = V_a^+ - V_a^- \qquad \text{(B24)}$$

where r_a and r_p are the apogee and perigee radii of the retro burnout elliptical orbit, respectively. From (B24) it follows that

$$\frac{\partial \Delta V_a}{\partial \bar{x}} = -\frac{Gm_e r_f}{v_a^+}\left[\frac{2r_a + r_f}{r_a^2(r_a + r_f)^2}\right]\frac{\partial r_a}{\partial \bar{x}}$$

$$-\frac{Gm_e}{v_a^-}\left[\frac{1}{(r_a + r_p)^2}\frac{\partial r_p}{\partial \bar{x}} - \frac{r_p(2r_a + r_p)}{r_a^2(r_a + r_p)^2}\frac{\partial r_a}{\partial \bar{x}}\right] \qquad \text{(B25)}$$

where $\bar{x}$ stands for either $\bar{r}$ or $\bar{v}$. Also,

$$\frac{\partial r_a}{\partial \bar{r}} = \frac{-\frac{\bar{v} \times \bar{h}}{Gm_e} + \left(\frac{r_a}{r}\right)^2 \hat{r}}{e} \qquad \text{(a)}$$

$$\frac{\partial r_p}{\partial \bar{r}} = \frac{\frac{\bar{v} \times \bar{h}}{Gm_e} - \left(\frac{r_p}{r}\right)^2 \hat{r}}{e} \qquad \text{(b)}$$

$$\frac{\partial r_a}{\partial \bar{v}} = \frac{-\bar{h} \times \bar{r} + r_a^2 \bar{v}}{eGm_e} \qquad \text{(c)}$$

$$\frac{\partial r_p}{\partial \bar{v}} = \frac{\bar{h} \times \bar{r} - r_p^2 \bar{v}}{eGm_e} \qquad \text{(d)}$$

where r is the retro burnout radius.

REFERENCES

1. Pontryagin, L. S., Boltyanskii, V. G., Gamkrelidze, R. V., and Mischenko, E. F. (K. N. Trirogoff, trans.), The Mathematical Theory of Optimal Processes, Interscience Publishers, New York, 1962.

2. Teren, F. and Spurlock, O. F., "Optimal Three Dimensional Launch Vehicle Trajectories with Attitude Rate Constraints," TN D-5117, 1969, NASA, Cleveland, Ohio.

3. Spurlock, O. F. and Teren, F., "Optimum Trajectories to Circular Synchronous Equatorial Orbit for Smaller-Than-Optimum Apogee Motors," TN D-5998, 1970, NASA, Cleveland, Ohio.

TABLE I. - COMPARISON OF PAYLOAD CAPABILITIES DETERMINED BY EXACT AND APPROXIMATE METHODS. SPECIFIC IMPULSE, I, 444 SECONDS

TTT, hrs	TAT, min	α	MF	C_3, km^2/sec^2	Normalized payload mass, m_{pl}/m_0		
					Exact	Approximate	Difference
24	3	1.0	0.87	15	0.1227	0.1227	0.0000
24	6	1.0	.87	15	.1287	.1287	.0000
24	6	1.0	.90	15	.2108	.2108	.0000
24	6	1.0	.90	5	.2937	.2936	.0001
12	3	0.3	.90	25	.1003	.1003	.0000
12	0	0.3	.90	25	.1121	.1119	.0002

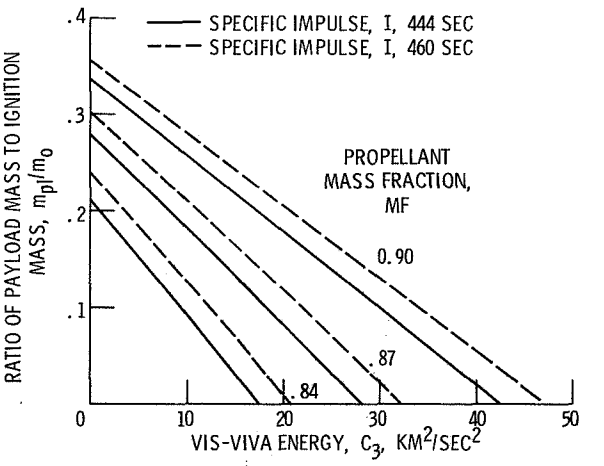

Figure 1. - Ideal performance capability. Ignition thrust-to-weight ratio, α, infinite; total trip time, TTT, zero; turn-around time, TAT, zero.

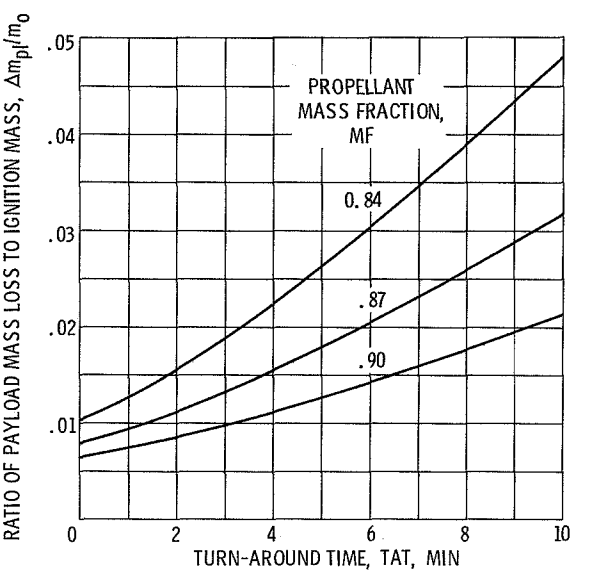

Figure 2. - Effect of turn-around time. Ignition thrust-to-weight ratio, α, 0.5; specific impulse, I, 444 seconds; vis-viva energy, C_3, 15 kilometers squared per second squared; total trip time, TTT, 24 hours.

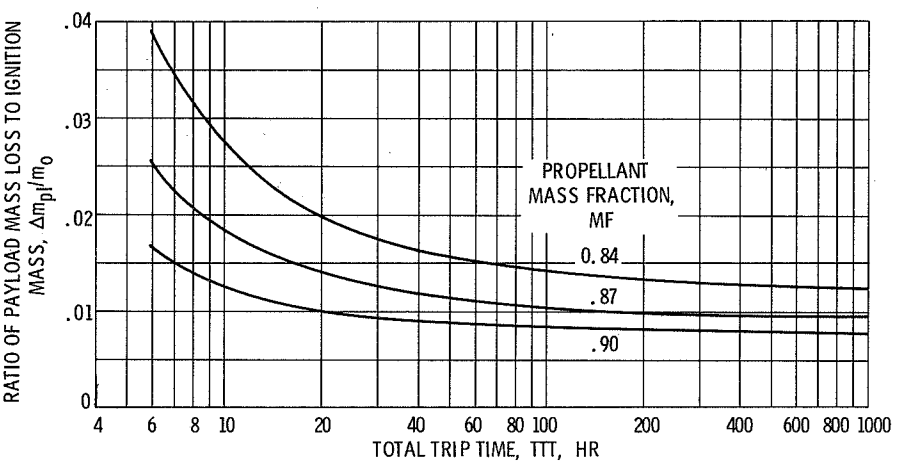

Figure 3. - Effect of total trip time. Ignition thrust-to-weight ratio, α, 0.5; specific impulse, I, 444 seconds; vis-viva energy, C_3, 15 kilometers squared per second squared; turn-around time, TAT, 3 minutes.

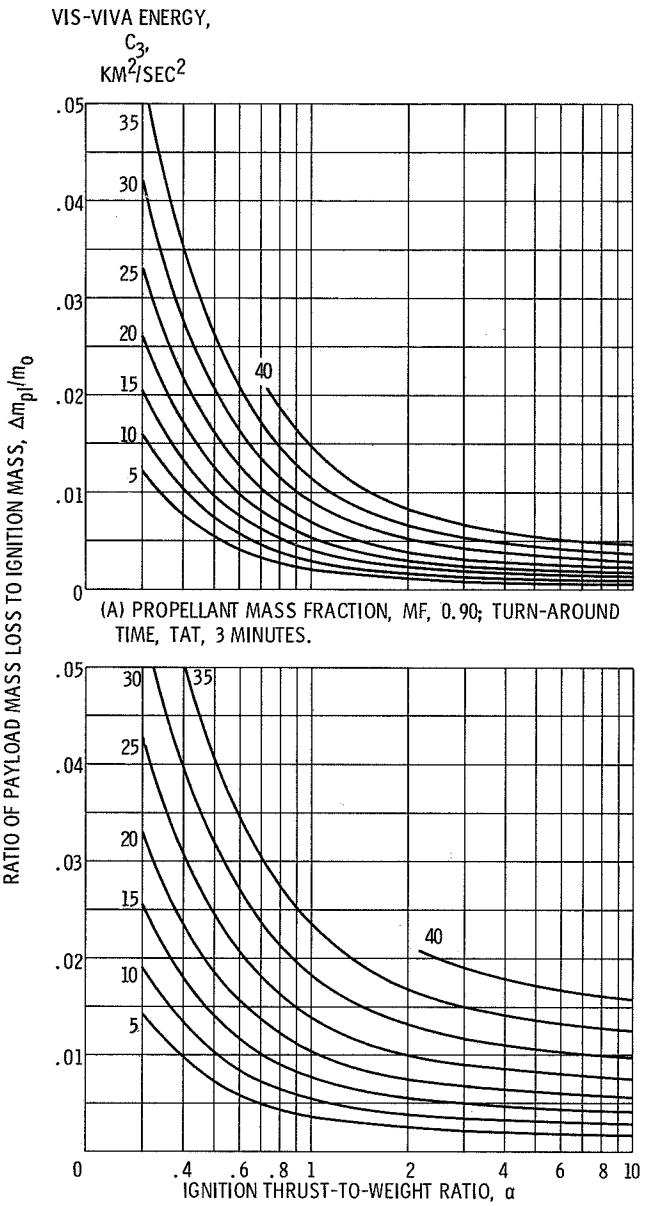

(A) PROPELLANT MASS FRACTION, MF, 0.90; TURN-AROUND TIME, TAT, 3 MINUTES.

(B) PROPELLANT MASS FRACTION, MF, 0.90; TURN-AROUND TIME, TAT, 6 MINUTES.

Figure 4. - Payload loss as a function of thrust-to-weight ratio. Specific impulse, I, 444 seconds; total trip time, TTT, 24 hours.

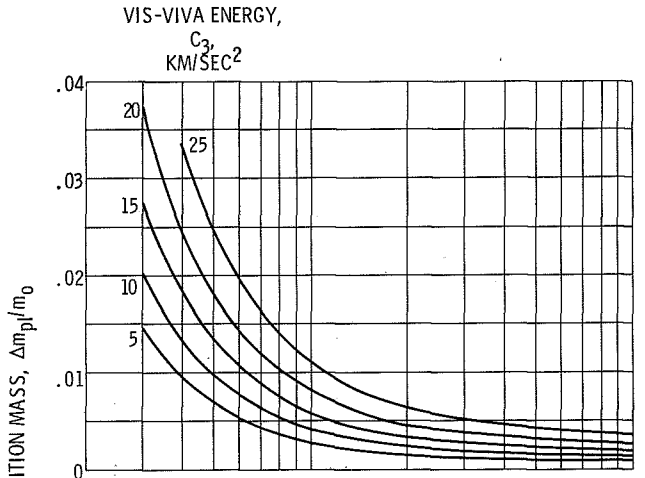

(C) PROPELLANT MASS FRACTION, MF, 0.87; TURN-AROUND TIME, TAT, 3 MINUTES.

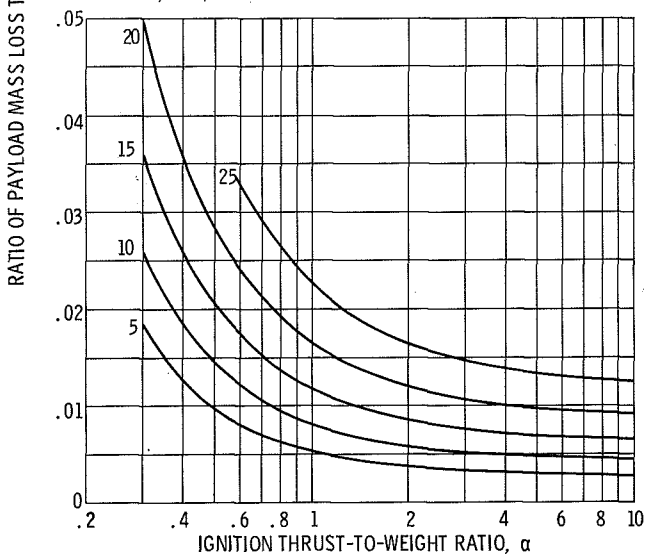

(D) PROPELLANT MASS FRACTION, MF, 0.87; TURN-AROUND TIME, TAT, 6 MINUTES.

Figure 4. - Continued.

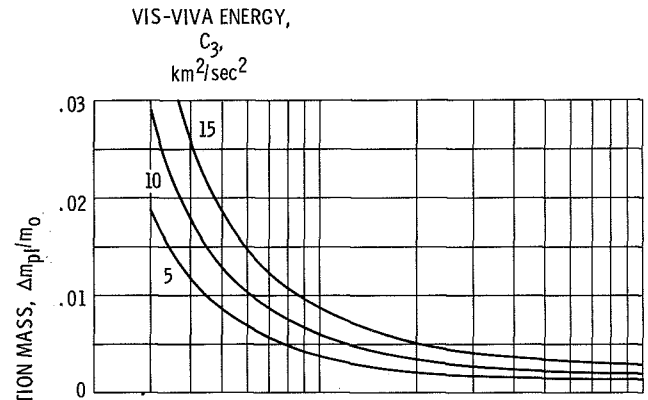

(E) PROPELLANT MASS FRACTION, MF, 0.84; TURN-AROUND TIME, TAT, 3 MINUTES.

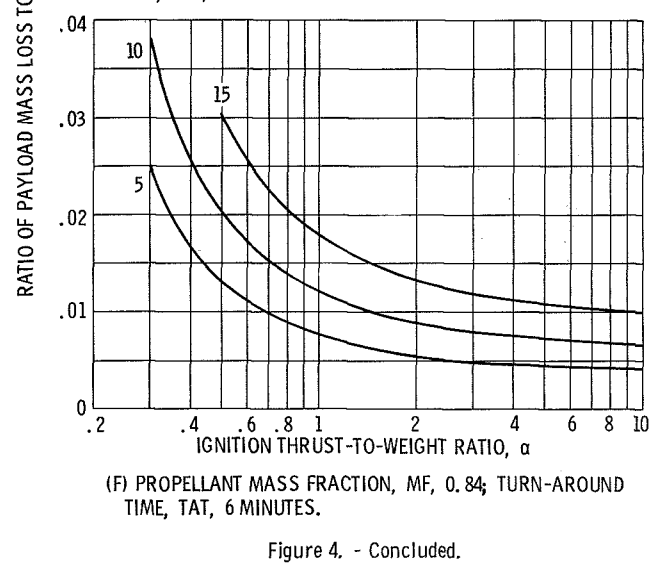

(F) PROPELLANT MASS FRACTION, MF, 0.84; TURN-AROUND TIME, TAT, 6 MINUTES.

Figure 4. - Concluded.

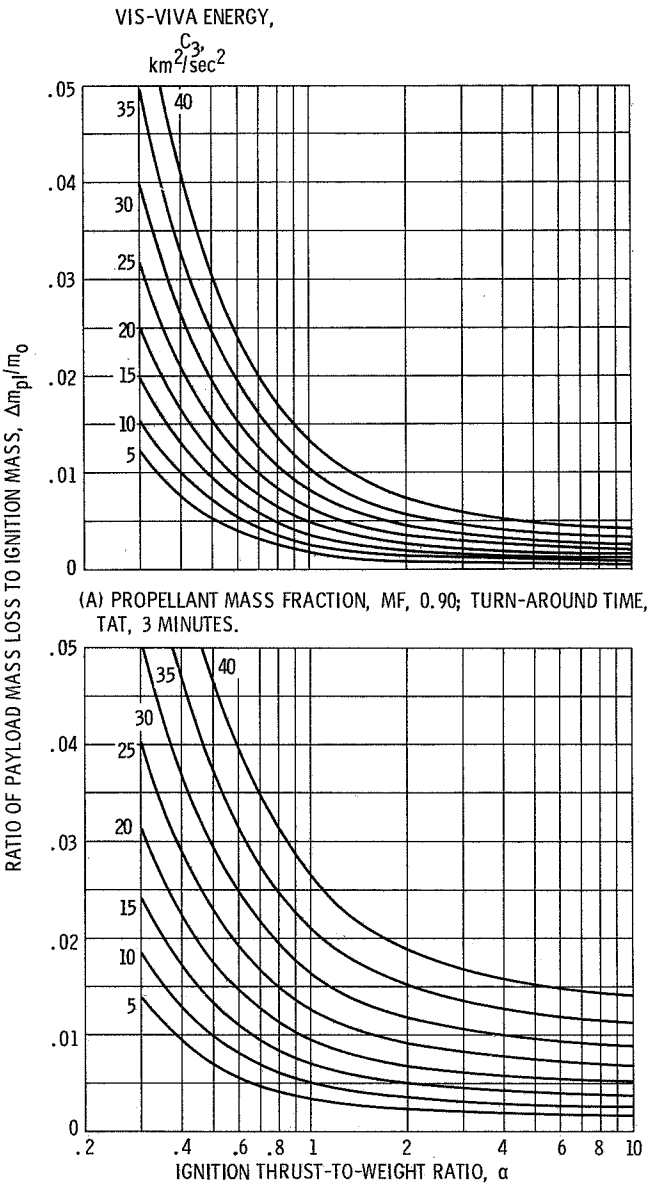

(A) PROPELLANT MASS FRACTION, MF, 0.90; TURN-AROUND TIME, TAT, 3 MINUTES.

(B) PROPELLANT MASS FRACTION, MF, 0.90; TURN-AROUND TIME, TAT, 6 MINUTES.

Figure 5. - Payload loss as a function of thrust-to-weight ratio. Specific impulse, I, 460 seconds; total trip time, TTT, 24 hours.

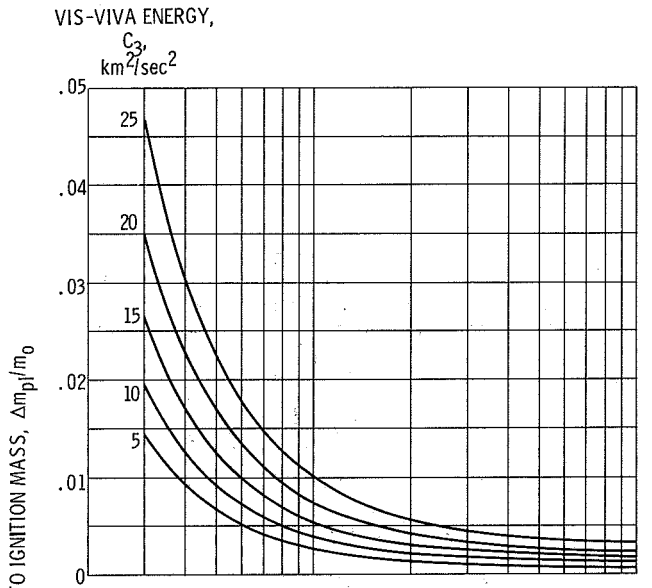

(C) PROPELLANT MASS FRACTION, MF, 0.87; TURN-AROUND TIME, TAT, 3 MINUTES.

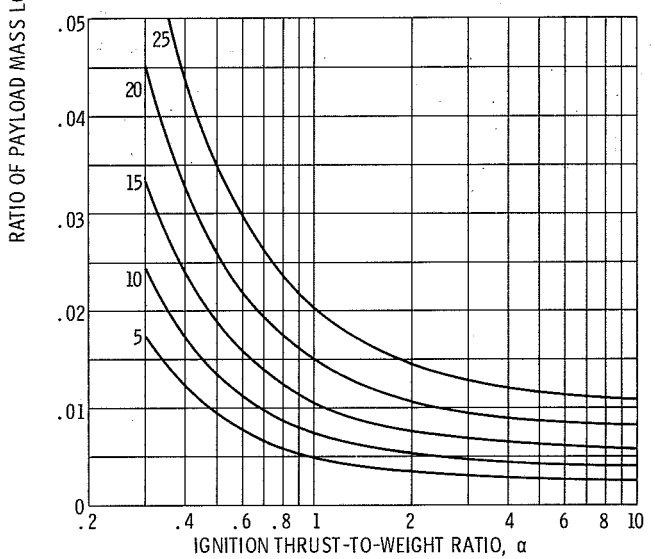

(D) PROPELLANT MASS FRACTION, MF, 0.87; TURN-AROUND TIME, TAT, 6 MINUTES.

Figure 5. - Continued.

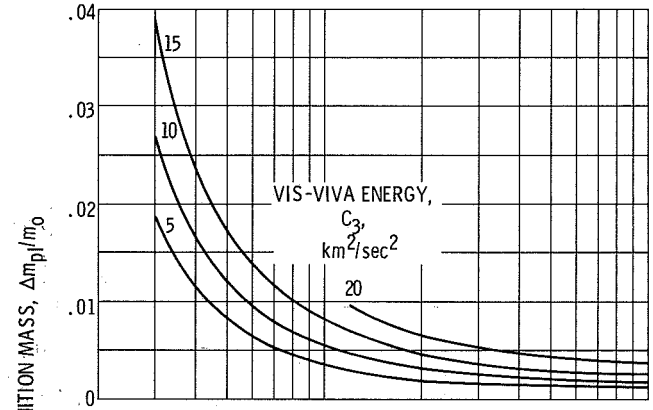

(E) PROPELLANT MASS FRACTION, MF, 0.84; TURN-AROUND TIME, TAT, 3 MINUTES.

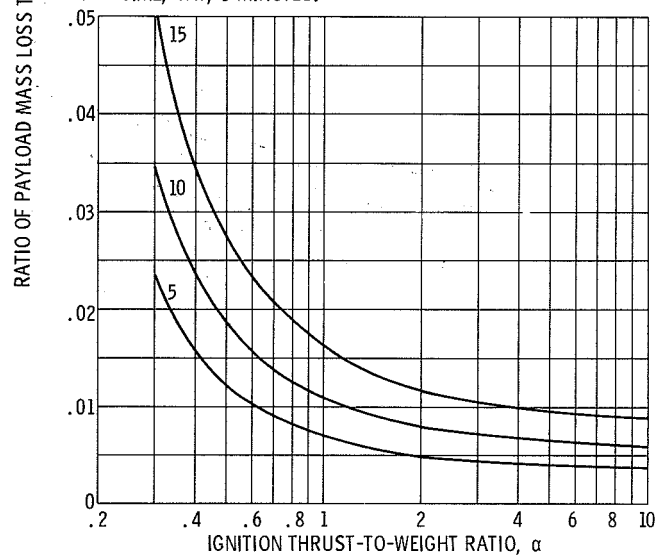

(F) PROPELLANT MASS FRACTION, MF, 0.84; TURN-AROUND TIME, TAT, 6 MINUTES.

Figure 5. - Concluded.

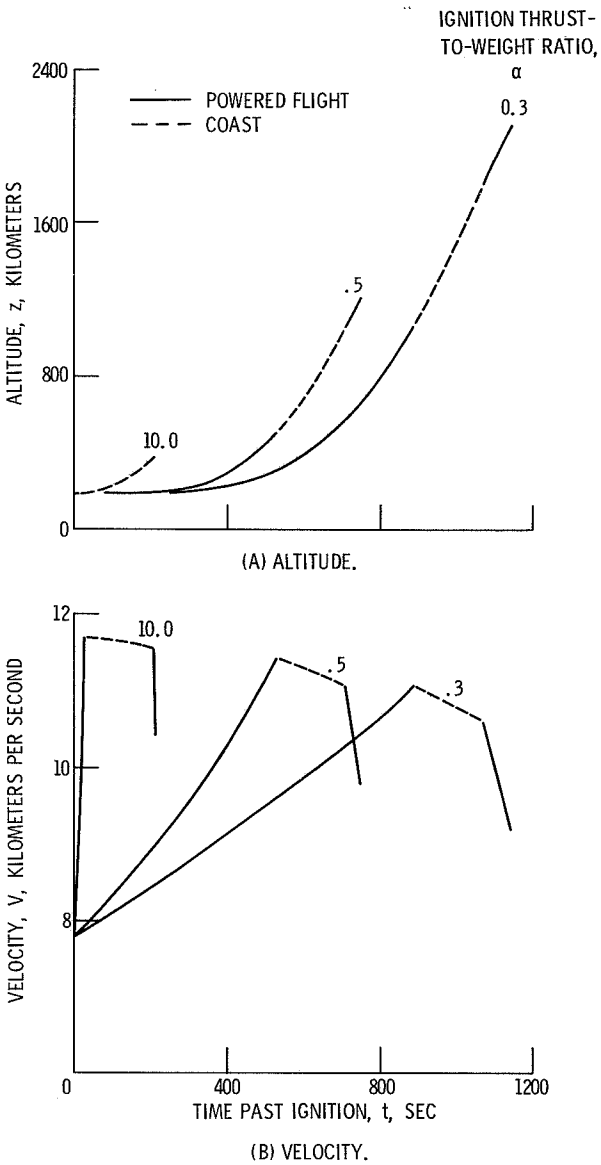

Figure 6. - Time history of various trajectory parameters for selected ignition thrust-to-weight, α, values. Specific impulse, I, 444 seconds; total trip time, TTT, 24 hours; turn-around time, TAT, 3 minutes; propellant mass fraction, MF, 0.90; vis-viva energy, C_3, 15 kilometers squared per second squared.

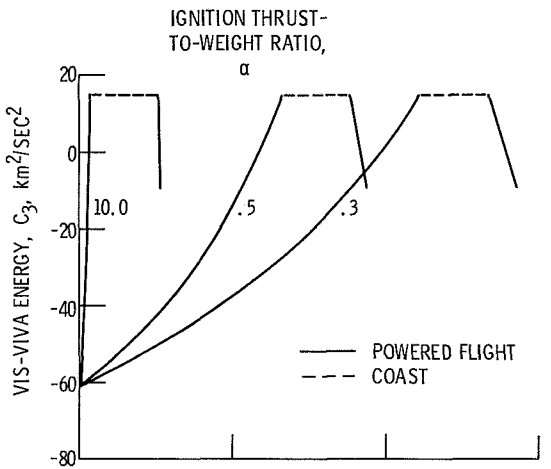

(C) VIS-VIVA ENERGY.

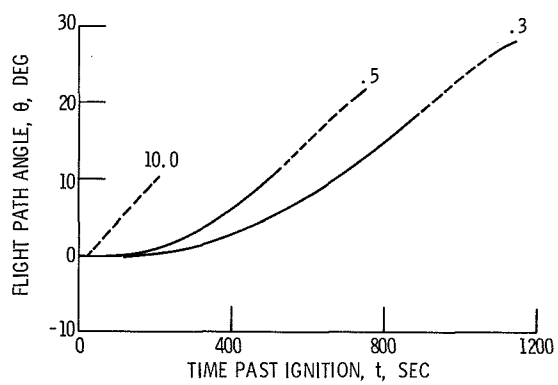

(D) FLIGHT PATH ANGLE.

Figure 6. - Continued.

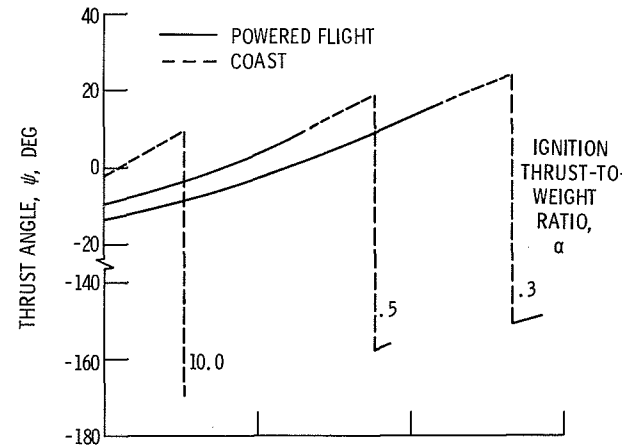

(E) THRUST ANGLE.

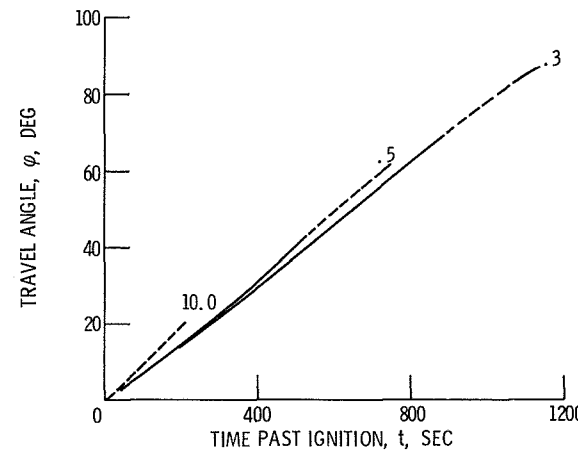

(F) TRAVEL ANGLE.

Figure 6. - Concluded.

E-6478

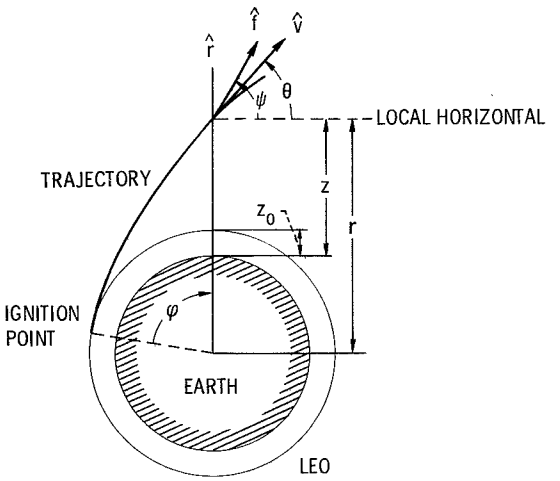

Figure 7. - Definition of problem variables.

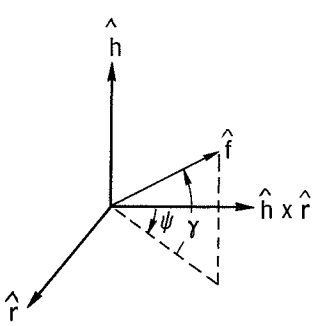

Figure 8. - Vehicle pitch and yaw attitudes.